Scaling of the velocity fluctuations in turbulent channels up to $Re_\tau = 2003$

By Sergio Hoyas AND Javier Jiménez
School of Aeronautics, U. Politécnica, 28040 Madrid, SPAIN

1. Numerical experiment

A direct simulation of a plane turbulent channel has been performed in a computational box with streamwise and spanwise periodicities $L_x = 8\pi h$ and $L_z = 3\pi h$, at a Reynolds number $Re_\tau = 2003$ based on the friction velocity u_τ and on the channel half-width h. It is therefore comparable with previous simulations at lower Reynolds numbers by our group (Del Álamo & Jiménez 2003; Del Álamo *et al.* 2004). We integrate evolution equations for the wall-normal vorticity ω_y and for the Laplacian of the wall-normal velocity $\phi = \nabla^2 v$, as in Kim, Moin & Moser (1987). The streamwise and spanwise coordinates are x and z, and the corresponding velocity components are u and w. The spatial discretization uses dealiased Fourier expansions in x and z, and seven-point compact finite differences in y, with fourth-order consistency and extended spectral-like resolution (Lele 1992). The temporal discretization is third-order semi-implicit Runge-Kutta (Spalart, Moser & Rogers 1991). The details of the code and of the parallelization strategy, as well as a fuller analysis of the results, will be the subject of future publications. Here we restrict ourselves to the description of the low-order statistics and to the discussion of the scaling of the velocity fluctuation intensities in the newly extended range of Reynolds numbers.

Table 1 summarizes the parameters of the present simulation, together with those of the previous ones used for comparison. It uses $N_x = 6144$, $N_y = 633$, $N_z = 4608$ collocation points. The simulation ran for about 6×10^6 processor-hours in 2048 processors of the Marenostrum computer at the Barcelona supercomputing center and generated approximately 25 TB of raw data. The wall-normal grid spacing is adjusted to keep the resolution ($\Delta y = 1.5\eta$) approximately constant in terms of the local isotropic Kolmogorov scale $\eta = (\nu^3/\varepsilon)^{1/4}$. It is slightly better in that respect than those of the lower Reynolds numbers. At the center of the channel the resolutions along the three coordinates are approximately equal ($\eta - 1.8\eta$), comparable to those of well-resolved simulations of isotropic turbulence (Jiménez *et al.* 1993). The microscale Reynolds number at that location is $Re_\lambda \approx 94$. The running times are given in terms of turnover periods for eddies of size h and of velocity u_τ. For the present box they are roughly equivalent to flow-throughs. The r.m.s. differences between one-point statistics over the first and second halves of the run are of the order of 1%, and the asymmetry of the profiles is of the same order.

2. Results

The mean velocity profile is shown in Fig. 1(*a*) in terms of the inverse Kármán 'constant' $y\partial_y U^+$, where U^+ is the mean velocity in wall units. This parameter is nowhere constant, but that is also the case for the high-Reynolds-number pipe data by McKeon *et al.* (2004) included for comparison, and for other experimental data not included in the figure. This is obviously the effect of the higher-order terms usually included in the

	Re_τ	Δx^+	Δz^+	Δy^+_{max}	L_x/h	L_z/h	tu_τ/h
▽ (Del Álamo & Jiménez 2003)	550	8.9	4.5	6.7	8π	4π	12.0
△ (Del Álamo *et al.* 2004)	934	9.2	3.8	7.6	8π	3π	8.5
○ , Present	2003	8.2	4.1	8.9	8π	3π	10.3

TABLE 1. Summary of cases. The resolution is measured in collocation points, and the symbols are used in the figures.

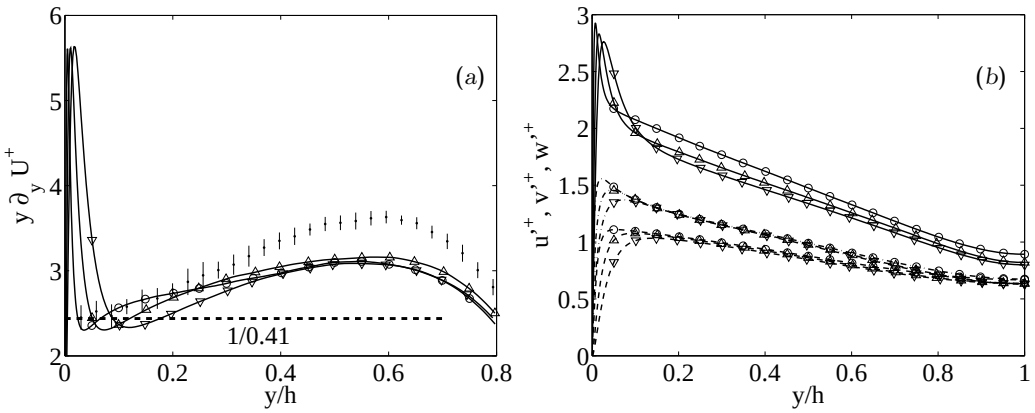

FIGURE 1. (a) Inverse Kármán constant. Symbols as in table 1. Dots with error bars are pipes from McKeon *et al.* (2004), with $Re_\tau > 2000$. (b) Velocity fluctuation intensities, in wall units. ——— , u'; - - - - , v'; —·— , w'.

'wake' component of the profile. However the minimum is reached in all the numerical cases around $y^+ = 50$, thereby calling into question the possibility, or even the relevance, of estimating the extent of the logarithmic layer in this way. If we take the usual estimate that $y^+ > 100$ and $y/h < 0.2$, the present simulation has a logarithmic region extending over a factor of 4. We will see below that there is a sizable part of the channel over which some length scales are approximately proportional to the wall distance y.

The r.m.s. velocity fluctuation profiles are shown in Fig. 1(b). None of them collapses exactly in wall units.

In the case of the transverse components, v' and w', the effect is weak. The three cases collapse well near the wall except within the buffer layer, where viscous effects are important. To our knowledge, the presence of a peak in the spanwise component had not been described before, and it is unclear whether it would tend to a finite limit at infinite Reynolds numbers. Away from the wall there is a weak tendency for v' and w' to increase with increasing Reynolds number, most noticeably at the center of the channel. Experimental data in pipes and channels (not shown) lend some support to that trend, although the scatter is large and values tend to cluster by facility rather than by Reynolds number.

The clearest effect is in the streamwise intensity u', which neither collapses near the wall nor far from it. The scaling failure near the wall was first reported in boundary layers by De Graaff & Eaton (2000), but there is no general agreement on its causes, and the authors of that article made the explanation a challenge for active theoreticians. The available data are collected in Fig. 2. The intensity in the near-wall peak, which

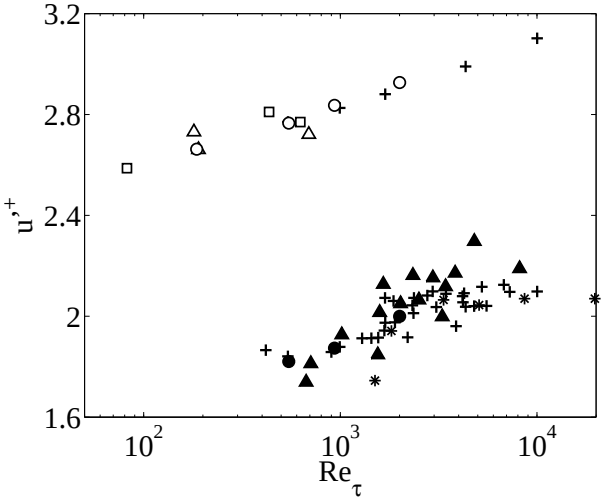

FIGURE 2. Streamwise fluctuation intensities from various sources. Open symbols, near-wall maximum; closed symbols, $y/h = 0.15$, $y^+ > 60$. □ , Couette flows; △ , pipes and channels; *, pipes from Morrison et al. (2004); +, boundary layers; ○ , present numerical channels.

is always achieved around $y^+ = 15$, increases steadily with the Reynolds number. The numerical cases confirm this trend. Any failure of near-wall scaling must come from the interaction of near-wall modes that scale in wall units with modes residing away from the wall, for it is only in that way that the Reynolds number is defined. The best-known proposal involves wall-parallel large-scale modes that reach the wall without being constrained by impermeability (Townsend 1976). It was suggested by Del Álamo & Jiménez (2003), on the basis of lower-Reynolds-number simulations, that the important outer modes were global ones spanning the whole channel and scaling with the boundary layer thickness. Hites (1997), among others, also described the near-wall spectrum in terms of the interaction of 'inner' and 'outer' energy peaks. The discussion of whether the data sustain such 'two-scale' models is the subject of most of the rest of this note.

The behavior of the intensities in the logarithmic layer is also included in Fig. 2, but it is less clear. There is a general growing trend, also shared by the numerics, but it could be argued that boundary layers saturate above $Re_\tau \approx 3000$, and Morrison et al. (2004) have concluded the same for pipes. That experiment is plotted separately for emphasis. The subject has been discussed for example in Del Álamo *et al.* (2004). However, except to present the additional data point in this figure, it will not be further discussed here.

Two-dimensional spectral energy densities at the height of the near-wall kinetic energy maximum are shown in Fig. 3. Two isolines are given for each case, representing the high-intensity core of the spectrum and its outer border. They confirm the results of simulations at lower Reynolds numbers in Del Álamo & Jiménez (2003). The core isolines scale well in wall units. Because the kinetic energy is the integral of the spectrum, this part of the energy also scales in wall units. The scaling failure appears for u and w in the upper right-hand corner, where a spectral ridge extends roughly along $\lambda_z = 0.15\lambda_x$. The ridge gets longer as the Reynolds number increases, reaching up to $\lambda_x \approx 10h$ in the case of ϕ_{uu}. The eddies in this ridge are inactive in the sense of Townsend (1976). They are not found in the v spectrum, nor in the Reynolds stress co-spectra in figure 3(c).

The vertical structure of the eddies responsible for the inactive ridge is shown in

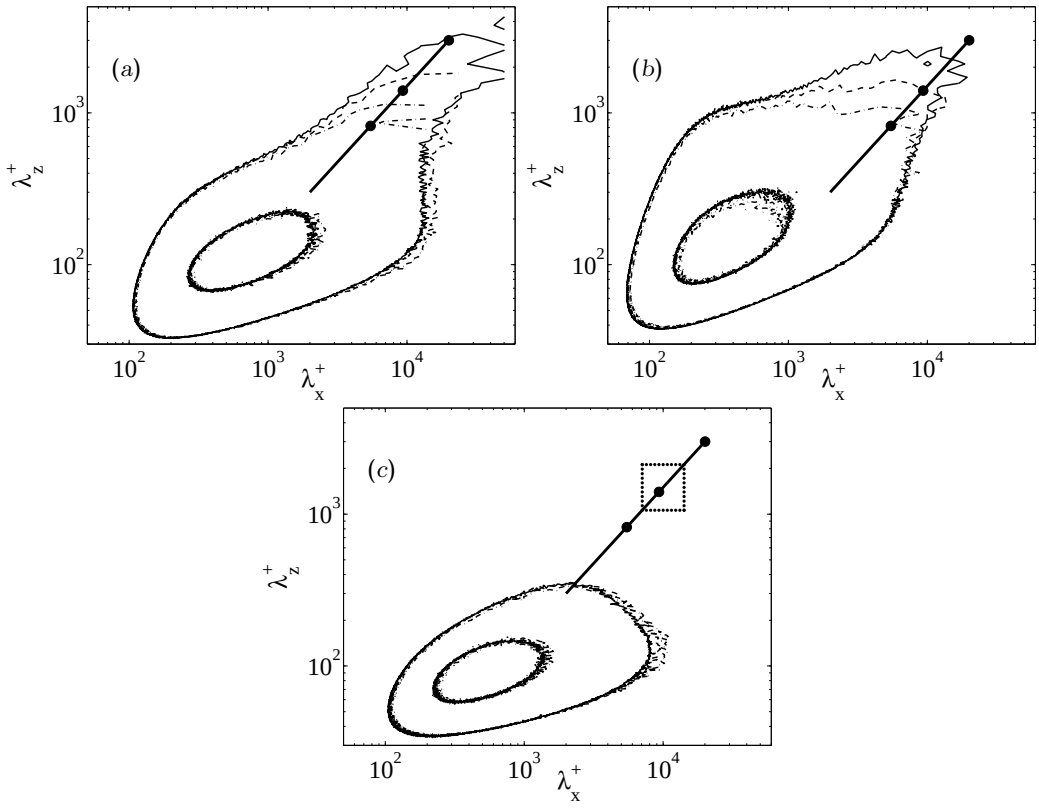

FIGURE 3. Spectral energy densities $\phi = k_x k_z E(k_x, k_z)$ at $y^+ = 15$, in terms of the wavelengths $\lambda = 2\pi/k$. (a) ϕ_{uu}. (b) ϕ_{ww}. (c) Cospectrum $-\phi_{uv}$. —·— , $Re_\tau = 550$; - - - - , 934; ——— , 2003. Spectra are normalized in wall units, and the two contours for each spectrum are 0.125 and 0.625 times the maximum of the spectrum for the highest Reynolds number. The heavy straight line is $\lambda_z = 0.15\lambda_x$, and the heavy dots are $\lambda_x = 10h$ for the three cases. The dotted rectangle in (c) is an example of the filtering boxes used to isolate the energies in Fig. 4.

Fig. 4(a), which shows contours of u'^2 integrated over logarithmic boxes of wavelengths centered along the ridge, with a fixed ratio between their longest (widest) and shortest (narrowest) wavelengths (see Fig. 3c for an example). The energy at the shortest boxes is concentrated near the wall. They fall in the core part of the spectrum, and they correspond to the classical buffer-layer streaks. It follows from Fig. 3(c) that these structures are active and carry Reynolds shear stress. On the basis of lower Reynolds number simulations, Jiménez, del Álamo & Flores (2004) hypothesized that the streaks are intrinsically infinitely long, but that they are truncated by the action of outer layer turbulence. This is now seen not to be the case. The 'wall modes' have a definite length – of the order of 10^4 wall units – that is independent of the Reynolds number. The ridge modes form a continuum that links those inner structures with the ones scaling in outer units. Figure 4(a) also contains a line joining the position of the maxima of the individual filtered energy profiles. The longer modes peak farther from the wall, and the locations of their peaks grow linearly as $y_{max} \approx \lambda_x/40 = \lambda_z/6$. Note that the locations of the peaks are within the nominal logarithmic layer and that they agree for the two Reynolds numbers for which a comparison is possible.

Even if the eddies along the spectral ridge are inactive near the wall, the same is not

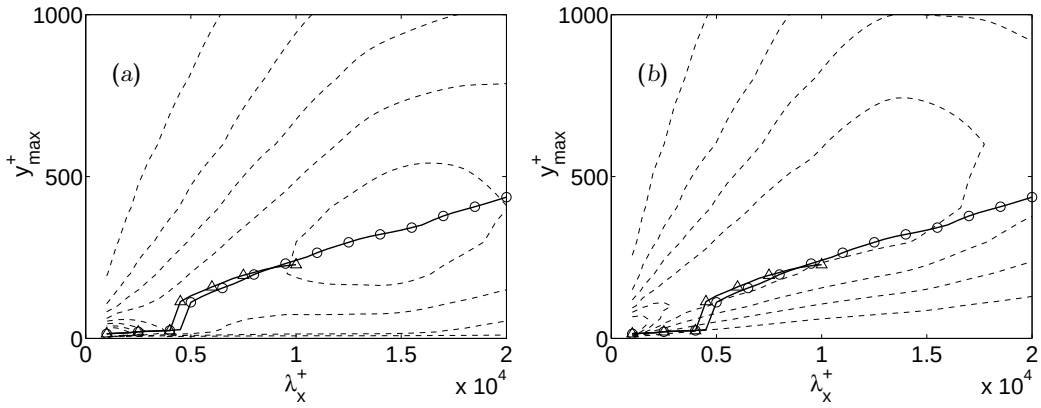

FIGURE 4. Contour plots of the spectral energy summed over logarithmic boxes of width 2, centered along $\lambda_z = 0.15\lambda_x$, such as the one in Fig. 2, as a function of y and of λ_x at the box center. $Re_\tau = 2003$. (a) Streamwise velocity fluctuations. Contours are 0.04(0.0.4)0.32. (b) Shear stress co-spectrum. Contours are 0.01(0.01)0.06. In both case the solid lines with symbols are the y positions of the maxima of the profiles in (a). Symbols as in table 1.

true at the levels where their intensities peak. That is seen in Fig. 4(b), which shows isocontours of the box-filtered Reynolds stress $-u'v'$. The ridge modes become more intense and more active as they grow larger, and they actually constitute the dominant modes within the logarithmic layer. The highest contours in the outer part of both Figs. 4(a) and 4(b) are comparable to the corresponding intensities in the buffer layer at the core of the u spectrum.

If we interpret λ_z as a width and y_{max} as a vertical semiaxis, the cross sections of the eddies would be oblate ellipses with aspect ratios of 3:1. Because of the linear growth of both quantities, the eddies can be visualized as conical. In that interpretation, the inclination of their axes would be $\arctan(1/40) \approx 1.5°$, although it is clear from Fig. 4(a) that the eddies are not symmetric and that any identification method based on integral quantities would result in somewhat higher angles. The inclination of the upper branches of the isocontours in both figures is approximately $10 - 12°$, which is of the order of the angles measured for the velocity correlation in experimental boundary layers (Krogstad & Antonia 1994; Christensen & Adrian 2001).

3. Conclusions

In summary, we have presented a new simulation of a turbulent channel containing an appreciable logarithmic layer, at a Reynolds number higher than those currently available. Several features in the logarithmic layer have been shown to grow linearly with wall distance, as in the classical scaling of the overlap region. The scaling failure of the intensity at the near-wall kinetic energy peak has been shown to be the result of eddies conforming to Townsend's inactive model, restricted at that wall distance to a spectral ridge of long and wide structures that is clearly distinguishable from the near-wall streaks. The latter scale well in wall units. The ridge modes are the near-wall footprints of eddies whose maximum intensities lie in the logarithmic region, and they link the near-wall streaks with the global modes identified elsewhere. They are inactive at the wall, but they support most of the Reynolds shear stresses at the location of their peaks.

Acknowledgments

This work was supported in part by the CICYT contract DPI2003-03434, by a generous grant of computer time from the Barcelona Supercomputing Center, and by an equally generous grant of mass storage by the Port d'Informació Científica (PIC). SH was supported in part by a Juan de la Cierva fellowship of the Spanish ministry of education. The stay of JJ at the CTR was supported in part by the Department of Energy under the ASC program.

REFERENCES

Del Álamo, J.C. & Jiménez, J. 2003 Spectra of very large anisotropic scales in turbulent channels, *Phys. Fluids* **15**, L41–L44.

Del Álamo, J.C., Jiménez, J., Zandonade, P. & Moser, R.D. 2004 Scaling of the energy spectra of turbulent channels, *J. Fluid Mech.* **500**, 135–144.

Christensen, K. T. & Adrian, R.J. 2001 Statistical evidence of hairpin vortex packets in wall turbulence, *J. Fluid Mech.* **431**, 433–443.

De Graaff, D. B. & Eaton, J. K. 2000 Reynolds-number scaling of the flat-plate turbulent boundary layer, *J. Fluid Mech.* **422**, 319–346.

Hites, M. 1997 Scaling of high-Reynolds number turbulent boundary layers in the National Diagnostic Facility, *PhD thesis*, Illinois Inst. of Technology.

Jiménez, J., del Álamo, J.C. & Flores, O. 2004 The large-scale dynamics of near-wall turbulence, *J. Fluid Mech.* **505**, 179–199.

Jiménez, J., Wray, A.A., Saffman, P.G. & Rogallo, R.S. 1993 The structure of intense vorticity in isotropic turbulence, *J. Fluid Mech.* **255**, 65–90.

Kim, J., Moin, P. & Moser, R.D. 1987 Turbulence statistics in fully developed channel flow at low Reynolds number, *J. Fluid Mech.* **177**, 133–166.

Krogstad, P.-A. & Antonia, R.A. 1994 Structure of turbulent boundary layers on smooth and rough walls, *J. Fluid Mech.* **277**, 1–21.

Lele, S.K. 1992 Compact finite differences schemes with spectral-like resolution, *J. Comp. Phys.* **174**, 510–551.

McKeon, B.J., Li, J., Jiang, W., Morrison, J.F. & Smits, A.J. 2004 Further observations on the mean velocity distribution in fully developed pipe flow, *J. Fluid Mech.* **501**, 135 – 147

Morrison, J. F., McKeon, B. J., Jiang, W. & Smits, A. J. 2004 Scaling of the streamwise velocity component in turbulent pipe flow, *J. Fluid Mech.* **508**, 99–131.

Spalart, P.R., Moser, R.D. & Rogers, M.M. 1991 Spectral method for the Navier–Stokes equations with one infinite and two periodic dimensions, *J. Comp. Phys.* **96**, 297–324.

Townsend, A.A. 1976 *The Structure of Turbulent Shear Flow.* Cambridge University Press.